Evidence of Sharp and Diffuse Domain Walls in $BiFeO_3$ by Means of Unit-Cell-Wise Strain and Polarization Maps Obtained with High Resolution Scanning Transmission Electron Microscopy

A. Lubk,[1,*] M. D. Rossell,[2] J. Seidel,[5] Q. He,[3] S. Y. Yang,[3] Y. H. Chu,[3,4] R. Ramesh,[3] M. J. Hÿtch,[1] and E. Snoeck[1]

[1]*CEMES-CNRS, Université de Toulouse, 29 rue Jeanne Marvig, 31055 Toulouse, France*

[2]*Electron Microscopy Center, Empa, Swiss Federal Laboratories for Materials Science and Technology, CH-8600 Dübendorf, Switzerland*

[3]*Department of Materials Science and Engineering, University of California, Berkeley, California 94720, USA*

[4]*Department of Materials Science and Engineering, National Chiao Tung University, Hsinchu 30010, Taiwan*

[5]*Materials Science Division, Lawrence Berkeley National Laboratory, Berkeley, California 94720, USA*

(Received 24 June 2011; published 25 July 2012)

Domain walls (DWs) substantially influence a large number of applications involving ferroelectric materials due to their limited mobility when shifted during polarization switching. The discovery of greatly enhanced conduction at $BiFeO_3$ DWs has highlighted yet another role of DWs as a local material state with unique properties. However, the lack of precise information on the local atomic structure is still hampering microscopical understanding of DW properties. Here, we examine the atomic structure of $BiFeO_3$ 109° DWs with pm precision by a combination of high-angle annular dark-field scanning transmission electron microscopy and a dedicated structural analysis. By measuring simultaneously local polarization and strain, we provide direct experimental proof for the straight DW structure predicted by *ab initio* calculations as well as the recently proposed theory of diffuse DWs, thus resolving a long-standing discrepancy between experimentally measured and theoretically predicted DW mobilities.

DOI: 10.1103/PhysRevLett.109.047601 PACS numbers: 77.80.Dj, 68.37.Ma, 77.55.fp, 77.80.Fm

Introduction.—$BiFeO_3$ is considered as an archetype multiferroic material, combining a particularly large ferroelectric polarization [1] with an antiferromagnetic spin configuration in a comparatively simple perovskite structure. In recent studies, increased conductivity [2] and photovoltaic effects [3] at $BiFeO_3$ DWs could be correlated to a small change of the lattice structure. According to Miller and Weinreich the mobility of ferroelectric DWs crucially depends on the formation of small rectangular steps at the DW eventually shifting the whole wall by growing parallel to the DW [Fig. 1(a)] [4]. However, the predicted DW mobilities from this model were one or two orders of magnitude too small. By means of extensive Monte Carlo simulations Shin *et al.* [5] showed that diffuse DW steps characterized by an inclined boundary with attenuated polarization in the surrounding resolve this discrepancy [Fig. 1(b)]. Such a diffuse configuration facilitates an easier switching of the polarization (hence larger step mobilities). It is also energetically favorable because the normal to the DW component of polarization is reduced by a factor of $1/\sqrt{2}$ at the step. An experimental proof of these so-called diffuse DWs could not be obtained so far. Mainly due to experimental restrictions (see Supplemental Material [6]), we focus on the connection between the detailed atomic structure and macroscopic electrical properties of the $BiFeO_3$ 109° DWs (and not 71° and 180° DWs) in the following.

High resolution transmission electron microscopy (HRTEM) has played a key role in determining the structure of ferroelectric DWs [2,7–9], because atomic positions and, via the Born effective charge tensor, also electric polarization can be determined at a unit-cell length scale. With the advent of Cs-corrected microscopes [10] the accuracy of these measurements was largely improved through a significant increase in resolution [11]. The benefit was particularly strong for the subdiscipline of high-angle annular dark-field scanning transmission electron microscopy (HAADF STEM) imaging [12], which has become a fully quantitative, chemically sensitive (Z dependent contrast), high resolution structure analysis tool

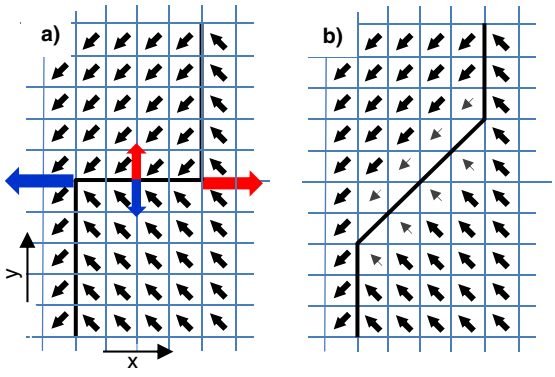

FIG. 1 (color online). Schematic of (a) Miller-Weinreich and (b) diffuse DW adapted from Shin *et al.* [5] to the case of $BiFeO_3$ 109° DW (see below). The black and gray arrows indicate the projected unit-cell-wise electric polarization **P**. A vertical shift of the steps into y ($-y$) direction denoted by small red (blue) arrows leads to a horizontal shift of the whole DW to the right (left) denoted by big red (blue) arrows.

[13]. Furthermore, model-based approaches to contrast evaluation [14,15] have proved particularly useful in reducing the influence of noise and extracting physical quantities like positions of atomic columns with a precision beyond the optical resolution of the microscope. Other microscopical techniques, e.g., electron holography, are not (yet) capable of determining polarization at unit-cell resolution, hence will not be considered in the following.

In this Letter, we use HAADF imaging performed at the TEAM 0.5 microscope in combination with a model-based structure determination optimized for large fields of view to precisely characterize the structure and polarization of $BiFeO_3$ 109° DWs with unprecedented precision and resolution.

BIFEO$_3$ *109° domain wall.*—At ambient conditions bulk $BiFeO_3$ is a rhombohedral perovskite ($a_{\mathrm{rh}} = 0.563$ nm, $\alpha_{\mathrm{rh}} = 59.35°$) incorporating 2 chemical units in one unit cell (see Supplemental Material [6]) [16]. Due to the almost cubic rhombohedral lattice angle $\alpha_{\mathrm{rh}} \approx 60°$, the lattice can be considered to be pseudocubic (indicated by $_{pc}$). At higher temperature and external pressure, e.g., introduced by a large lattice mismatch with the substrate, other phases have been identified (e.g., [17–19]).

A precise model structure for the 109° $BiFeO_3$ DW has been proposed by density functional calculations (DFT) [20]. It was observed that the alternating rotation pattern of the oxygen octahedra is continuous across the DW to minimize the DW energy. Secondly, and connected to the stiffness of this octahedra pattern, the Bi sublattice is predicted to change abruptly at the DW, whereas the iron sublattice within the oxygen octahedra remains rather constant [Fig. 2(c)]. The predicted DW width is two pseudocubic unit cells ($a_{pc} = 0.396$ nm). Within this DW extension the parallel component of the polarization changes sign whereas the normal component shows a small kink but otherwise remains constant. This small kink is responsible for a characteristic step of the electrostatic potential at the DW, which was proposed to play a role in the enhanced conductivity and photovoltaic effects measured at the wall [2]. Recent experimental studies confirmed the theoretically predicted DW width [8]; however, first experimental evidence for more subtle structural details like the Bi-sublattice jump is demonstrated below.

HAADF structure determination.—HAADF-STEM was carried out using the aberration-corrected TEAM 0.5 microscope [11] operated at 300 kV with a collection angle interval between 45–290 mrad in order to increase the signal from the light FeO atomic column. The probe convergence angle was adjusted to ~19 mrad in order to provide a sufficiently small probe size (60 pm) minimizing cross-talk between the atomic columns (see Supplemental Material [6]). Due to the limited dynamical range of the detection process and the presence of shot noise, the light O columns are not visible in $[100]_{pc}$ orientation above the

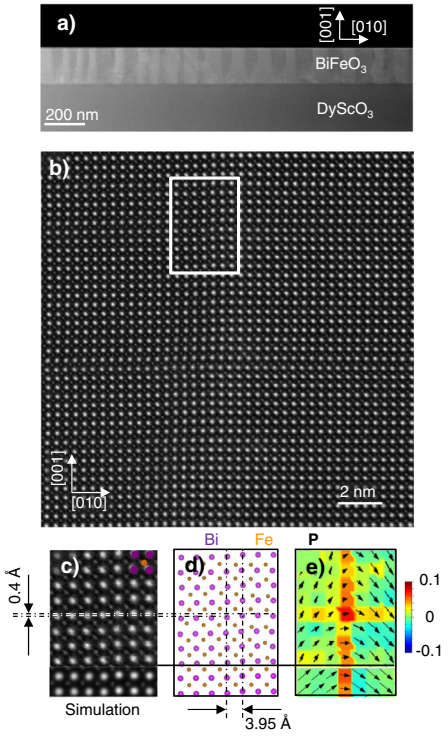

FIG. 2 (color online). Lattice analysis principle and 109° DW structure. (a) Overview of $BiFeO_3$ layer grown on $DyScO_3$. (b) Original HAADF image. (c) Enlarged rectangle (upper part) and simulated STEM image of DFT DW structure (lower part). (d) Fitted column positions and types (upper part) and the according DFT DW structure (lower part). (d) Unit cell wise shear (color) and electric polarization (arrows) obtained from the experimental (upper part) and simulated STEM image (lower part).

background intensity between the heavy Bi ($Z = 83$) and FeO ($Z = 26, 8$) columns. However, the indirect influence of O atoms can be significant in particular if different oxygen octahedra tilts are well separated in projection [8].

In order to determine the atomic structure in field of views containing several thousand atomic columns, we employed, a with respect to the peak height ordered, maximum-likelihood fit of a bivariate Gaussian plus background to each column, starting with the heavy Bi columns and proceeding with the light FeO columns (see Supplemental Material [6]). Already fitted column contrast are subtracted from the original image before proceeding with the next column fit; thus, FeO columns are correlated to previously determined Bi columns. This procedure ensures that the important problem of scattering at neighboring atomic columns, eventually obscuring the concept of uncorrelated HAADF column contrasts, is taken into account: By means of dynamic scattering simulations we show (see Supplemental Material [6]) that, in the particular case of $BiFeO_3$, the HAADF signal originating from neighboring columns only significantly contributes if the beam is centered on the light FeO column. If the beam is centered

on a heavy Bi column, the effect of channeling and the large difference in Z attenuates strongly an intermixing with other columns; hence, Bi columns can be safely fitted independently. According to Eq. (106) in Ref. [21] the column position fit error was estimated 5–7 pm (12–16 pm) in case of Bi (FeO).

Indeed, two important systematic errors surmount the statistical uncertainty in our measurement: (i) the scanning error introduces characteristic displacements up to 50 pm in x direction when jumping the beam to the next scanning line. These jump shifts can be identified and at least partially corrected (see Supplemental Material [6]). Additionally the DWs are aligned perpendicular to the scanning direction, rendering measurements of DW widths and change of Fe or Bi positions over the wall rather robust against the jump shift. (ii) Differing zone-axis misalignments and influence of coma on both sides of the DW can cause a systematic offset [$\mathcal{O}$(10 pm)] in the measured Bi-FeO distance. Indeed, a slight elliptic elongation of the observed column contrasts [Fig. 2(c)] corroborates the presence of this effect. We applied a phenomenological gauge based on symmetry arguments to correct this offset (see Supplemental Material [6]).

From the more precise Bi column positions $\mathbf{R}_{\mathrm{Bi}}$, the displacement field $\mathbf{u}(\mathbf{R}_{\mathrm{Bi,ref}}) = \mathbf{R}_{\mathrm{Bi}} - \mathbf{R}_{\mathrm{Bi,ref}}$ is obtained, with reference positions $\mathbf{R}_{\mathrm{Bi,ref}}$ being extrapolated by repeating a mean undisturbed pseudocubic unit cell observed far from the DW over the whole field of view. Now, engineering strain $\boldsymbol{\varepsilon}(\mathbf{R})$ and rigid lattice rotation $\Omega(\mathbf{R})$ follow from the usual definitions (see Supplemental Material [6]). Finally, we use the Fe displacement $\delta_{\mathrm{Fe}}(\mathbf{R}_{\mathrm{Bi,ref}}) = \mathbf{R}_{\mathrm{Fe}} - \mathbf{R}_{\mathrm{Bi}} - (0.5, 0.5)^T a_{pc}$ from the unit cell center as a measure for the electric polarization $\mathbf{P}(\mathbf{R}) = V_{uc}^{-1}\mathbf{Z}^*\boldsymbol{\delta}_{\mathrm{Fe}}(\mathbf{R})$, where $\mathbf{Z}^*$ is a special Born effective charge tensor (see Supplemental Material [6]).

Strain and polarization maps.—In the following, we show 109° DWs observed in an approximately 140 nm thick layer of pure $BiFeO_3$ which was epitaxially grown in $(001)_{pc}$ orientation on low miscut $DyScO_3(110)$ single crystal substrate ($a_{pc} = 0.3945$ nm) by pulsed laser deposition (670 °C at 100 mTorr of O_2, for more details see Supplemental Material [6]). In order to observe the $\{010\}_{pc}$-oriented 109° DWs [22] "edge-on", TEM samples in $[100]_{pc}$ zone-axis orientation were prepared in cross-section geometry applying liquid nitrogen cooled ion milling in the last stage to reduce specimen damage (Fig. 2 and Supplemental Material [6] for details). The images were obtained from quite thick areas (40 ± 5 nm, measured by using the electron energy loss spectroscopy based t/λ method [24]) of the film to ensure the film structure is not relaxed and the DW structure is not modified: several unit cells away from the DW we observed a pseudocubic structure ($\alpha_{pc} = 89.9° \pm 0.1°$) (also confirmed by XRD [25]). At high resolution, the 109° DW is characterized by an abrupt shift of the Bi sublattice in y direction (Fig. 2). The average experimentally observed shift of 0.4 Å is slightly below our *ab initio* predictions of 0.5 Å, which is, however, mainly a fitting effect (see below). The observed width of the DW extends over 2 pseudocubic unit cells with an expansion of the lattice parameter in x direction observable (in agreement with previous STM measurements [25]). The average rigid lattice rotation angle $\Delta\Omega$ between the left and the right hand side of all DWs investigated in this study is $0.6 \pm 0.1°$, which corresponds to a rhombohedral angle α of $59.6 \pm 0.1°$ slightly larger than the bulk value (see Supplemental Material [6] for the details) [16]. The small discrepancy to the pseudocubic structure observed far away from the DW can be attributed to measurement errors and a slight deviation of the thin film structure from bulk. In order to verify these results we performed dynamic scattering STEM imaging simulations at the complete DFT DW structure (including O positions) and repeated the fit on that simulated result. We obtain very good agreement between the input DFT structure and from STEM simulations or experimental images fitted positions [Figs. 2(c) and 2(e)]. E.g. the above mentioned Bi sublattice shift in y direction obtained from the simulated image is 0.4(4) Å almost perfectly matching the 0.4(2) Å found experimentally. To investigate the influence of strain on the DW, $Bi_{0.9}La_{0.1}FeO_3$ has been prepared and oriented similarly to the undoped ones (see Supplemental Material [6]). Here, the large La ions are expected to slightly push $BiFeO_3$ towards cubic symmetry, concomitantly reducing the lattice constant and the electric polarization [26]. Indeed, we find a reduced rigid lattice rotation angle of 0.37°, corresponding to a rhombohedral angle of 59.8°, and a electric polarization reduced roughly by a factor of two (see Supplemental Material [6]).

Furthermore, a set of DW steps, disrupting straight DW sections, was observed (Fig. 3 and Supplemental Material [6]). Because they always formed a staircase we attribute them to a frozen in motion of the DW like predicted by

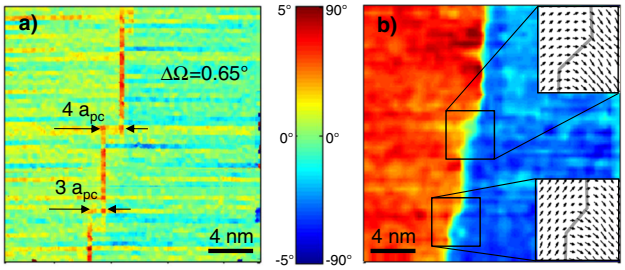

FIG. 3 (color online). (a) Lattice and (b) polarization rotation field at $BiFeO_3$ 109° DW containing steps. The comparatively large scatter in polarization angle is caused by the Fe-position error. In contrast to the lattice strain, the polarization vector field at the steps (enlarged squares) shows, on the length scale of the diagonal boundary, a diffuse rotation and attenuation.

the DW motion models (in contrast to a randomly bended DW with steps occurring in both directions). Shear and rigid lattice rotation indicate a 90° step morphology containing a short and slightly smeared (001)-oriented DW (indicated by arrows) in contrast to the sharp (010)-DW. The polarization, on the other hand, changes across a 45° inclined line [Fig. 3(b)] with the polarization vector mainly performing a slow rotation. We observed similar steps comprising 1 to 4 pseudocubic unit cells with a a preference for 2 pseudocubic units at a large variety of DWs (for 3 examples and the statistic see Supplemental Material [6]). We consider a 3D growth of the step in [100] direction as a possible yet implausible explanation for the observed strain and polarization variations for the following two reasons: (i) both strain and polarization would then smear out similarly in projection, but different from step to step depending on the particular 3D growth, which is not observed experimentally; (ii) the growth of bumps is only rarely observed at the straight section of the DW, indicating a small probability for such a morphology in [100] direction. Indeed, the observed polarization variation strikingly agrees with the proposed diffuse boundary DW model (Fig. 1). In addition, several features, which have not been considered in the theoretic model become visible: most notably, the polarization vector is both attenuated and rotated at the diffuse step [Fig. 3(b) insets]. Furthermore, the step height is determined by the bulk structure; i.e., we attribute the preference for a $2a_{pc}$ step height to the alternating oxygen octahedra tilts. This additional information is crucial for a quantitative modeling of DW motion in $BiFeO_3$, e.g., because depolarizing fields of a locally rotating polarization differ from a merely attenuated one. As the general mechanisms, e.g., depolarization field reduction, leading to the formation of diffuse DWs are independent from the particular type of DW, similar diffuse steps are expected at differently oriented DWs (e.g., 71°) or DWs in other materials (e.g., $PbTiO_3$). Substantial differences in DW mobilities, however, can now be explained by, e.g., a varying step height and diffuseness, depending on, e.g., local strain and polarization.

Summary.—We have used a combination of high resolution HAADF-STEM and a dedicated model-based structural analysis to provide unit-cell wise information on strain and polarization at $BiFeO_3$ 109° DW. It was demonstrated that the straight DW structure agrees in detail with previous *ab initio* predictions used to explain increased conductivity. ''Chemical pressure'' introduced by La doping was found to modify the DW angle in accordance with the rhombohedral lattice angle. Finally, we provided first experimental evidence, including detailed polarization profiles, for diffuse DWs proposed to explain experimentally found DW mobilities.

We highly appreciate Rolf Erni for useful discussions and stimulation. The authors acknowledge financial support from the European Union under the Framework 6 program under a contract for an Integrated Infrastructure Initiative. Reference 026019 ESTEEM. Part of this work was performed at the National Center for Electron Microscopy (LBNL) which is supported by the Office of Science, Office of Basic Energy Sciences of the U.S. Department of Energy under contract number DE-AC02-05CH11231.

*axel.lubk@yahoo.de

[1] G. Catalan and J. F. Scott, Adv. Mater. **21**, 2463 (2009).
[2] J. Seidel, L. W. Martin, Q. He, Q. Zhan, Y.-H. Chu, A. Rother, M. E. Hawkridge, P. Maksymovych, P. Yu, and M. Gajek *et al.*, Nature Mater. **8**, 229 (2009).
[3] S. Yang, J. Seidel, S. Byrnes, P. Shafer, C.-H. Yang, M. Rossell, P. Yu, Y.-H. Chu, J. Scott, and J. Ager *et al.*, Nature Nanotech. **5**, 143 (2010).
[4] R. C. Miller and G. Weinreich, Phys. Rev. **117**, 1460 (1960).
[5] Y.-H. Shin, I. Grinberg, I.-W. Chen, and A. M. Rappe, Nature (London) **449**, 881 (2007).
[6] See Supplemental Material at http://link.aps.org/supplemental/10.1103/PhysRevLett.109.047601 for detailed information on lattice structure, STEM imaging and structure analysis, measurement errors, growth conditions, and additional experimental evidence.
[7] S. Stemmer, S. K. Streiffer, F. Ernst, and M. Rühle, Philos. Mag. A **71**, 713 (1995).
[8] A. Borisevich, O. S. Ovchinnikov, H. J. Chang, M. P. Oxley, P. Yu, J. Seidel, E. A. Eliseev, A. N. Morozovska, R. Ramesh, and S. J. Pennycook *et al.*, ACS Nano **4**, 6071 (2010).
[9] C.-L. Jia, S.-B. Mi, K. Urban, I. Vrejoiu, M. Alexe, and D. Hesse, Nature Mater. **7**, 57 (2008).
[10] M. Haider, H. Rose, S. Uhlemann, E. Schwan, B. Kabius, and K. Urban, Ultramicroscopy **75**, 53 (1998).
[11] C. Kisielowski, B. Freitag, M. Bischoff, H. van Lin, S. Lazar, G. Knippels, P. Tiemeijer, M. van der Stam, S. von Harrach, and M. Stekelenburg *et al.*, Miscrosc. Microanal. Microstruct. **14**, 469 (2008).
[12] R. Erni, M. D. Rossell, C. Kisielowski, and U. Dahmen, Phys. Rev. Lett. **102**, 096101 (2009).
[13] J. M. LeBeau, S. D. Findlay, L. J. Allen, and S. Stemmer, Phys. Rev. Lett. **100**, 206101 (2008).
[14] S. Van Aert, J. Verbeeck, R. Erni, S. Bals, M. Luysberg, D. Van Dyck, and G. Van Tendeloo, Ultramicroscopy **109**, 1236 (2009).
[15] S. Van Aert, K. J. Batenburg, M. D. Rossell, R. Erni, and G. Van Tendeloo, Nature (London) **470**, 374 (2011).
[16] F. Kubel and H. Schmid, Acta Crystallogr. Sect. B **46**, 698 (1990).
[17] D. Ricinschi, K.-Y. Yun, and M. Okuyama, J. Phys. Condens. Matter **18**, L97 (2006).
[18] H. Béa, B. Dupé, S. Fusil, R. Mattana, E. Jacquet, B. Warot-Fonrose, F. Wilhelm, A. Rogalev, S. Petit, and V. Cros *et al.*, Phys. Rev. Lett. **102**, 217603 (2009).
[19] J. Wang, J. B. Neaton, H. Zheng, V. Nagarajan, S. B. Ogale, B. Liu, D. Viehland, V. Vaithyanathan, D. G. Schlom, and U. V. Waghmare *et al.*, Science **299**, 1719 (2003).
[20] A. Lubk, S. Gemming, and N. A. Spaldin, Phys. Rev. B **80**, 104110 (2009).

[21] A. J. den Dekker, S. Van Aert, A. van den Bos, and D. Van Dyck, Ultramicroscopy **104**, 83 (2005).
[22] Possible 71 and 180° DWs are $\{110\}_{pc}$-oriented.[23]
[23] S. K. Streiffer, C. B. Parker, A. E. Romanov, M. J. Lefevre, L. Zhao, J. S. Speck, W. Pompe, C. M. Foster, and G. R. Bai, J. Appl. Phys. **83**, 2742 (1998).
[24] T. Malis, S. C. Cheng, and R. F. Egerton, J. Electron Microsc. Tech. **8**, 193 (1988).
[25] Y.-H. Chu, Q. He, C.-H. Yang, P. Yu, L. W. Martin, P. Shafer, and R. Ramesh, Nano Lett. **9**, 1726 (2009), http://pubs.acs.org/doi/pdf/10.1021/nl900723j.
[26] V. Singh, A. Garg, and D. Agrawal, Appl. Phys. Lett., **92**, 152905 (2008).